Efficacy of the Janus kinase 1/2 inhibitor ruxolitinib in the treatment of vasculopathy associated with TMEM173-activating mutations in 3 children

DOI:
10.1016/j.jaci.2016.07.015

Document Version
Accepted author manuscript

Published in:
The Journal of allergy and clinical immunology

EFFICACY OF THE JANUS KINASE 1/2 INHIBITOR RUXOLITINIB IN THE TREATMENT OF VASCULOPATHY ASSOCIATED WITH *TMEM173*-ACTIVATING MUTATIONS IN THREE CHILDREN

Marie-Louise Frémond, MD,[a,b,c*] Mathieu Paul Rodero, PhD,[b,c*] Nadia Jeremiah, PhD,[b,d] Alexandre Belot, MD, PhD,[e,f] Eric Jeziorski, MD,[g] Darragh Duffy, PhD,[h,i] Didier Bessis, MD,[j] Guilhem Cros, MD,[a] Gillian I Rice, PhD,[k] Bruno Charbit, MSc,[h] Anne Hulin, PharmD, PhD,[l] Nihel Khoudour, MD,[l] Consuelo Modesto Caballero, MD,[m] Christine Bodemer, MD, PhD,[b,n] Monique Fabre, MD,[o] Laureline Berteloot, MD,[p] Muriel Le Bourgeois, MD,[q] Philippe Reix, MD,[r] Thierry Walzer, PhD,[f] Despina Moshous, MD, PhD,[a,b,s] Stéphane Blanche, MD, PhD,[a,b] Alain Fischer, MD, PhD,[a,b,t,u] Brigitte Bader-Meunier, MD,[a,b,d] Fréderic Rieux-Laucat, PhD,[b,d*] Yanick Joseph Crow, MD, PhD,[b,c,k*] Bénédicte Neven, MD, PhD,[a,b,d]

[a]Pediatric Hematology-Immunology and Rheumatology Department, Hôpital Necker-Enfants Malades, AP-HP, Paris, France

[b]Paris Descartes University, Sorbonne-Paris-Cité, Institut Imagine, Paris, France

[c]INSERM UMR 1163, Laboratory of Neurogenetics and Neuroinflammation, Paris, France

[d]INSERM UMR 1163, Laboratory of Immunogenetics of Pediatric Autoimmunity, Paris, France

[e]Pediatric Rheumatology, Nephrology and Dermatology Department, Hospices Civils de Lyon, Lyon, France

[f]CIRI, Centre International de Recherche en Infectiologie, INSERM, U1111, CNRS UMR5308, Ecole Normale Supérieure de Lyon, Université Lyon 1, Lyon, France

[g]Pediatrics Department, Centre Hospitalier Universitaire de Montpellier, Montpellier, France

[h]INSERM UMR 818, Laboratory of Dendritic Cell Immunobiology, Institut Pasteur, Paris, France

[i]Center for Human Immunology, Institut Pasteur, Paris, France

[j]Dermatology Department, Centre Hospitalier Universitaire de Montpellier, Montpellier, France

[k]Manchester Centre for Genomic Medicine, Institute of Human Development Faculty of Medical and Human Sciences, Manchester Academic Health Sciences Centre, University of Manchester, Manchester, United Kingdom

[l]Pharmacology and Toxicology Laboratory, Hôpital Universitaire Henri Mondor, Créteil, France

[m]Pediatric Rheumatology Department, Hospital Universitari Vall d'Hebron, Barcelona, Spain
[n]Dermatology Department, Hôpital Necker-Enfants Malades, AP-HP, Paris, France
[o]Pathology Department, Hôpital Necker-Enfants Malades, AP-HP, Paris, France
[p]Pediatric Radiology Department, Hôpital Necker-Enfants Malades, AP-HP, Paris, France
[q]Pediatric Pneumology Department, Hôpital Necker-Enfants Malades, AP-HP, Paris, France
[r]Pneumology Department, Centre de Référence de la Mucoviscidose, Hospices Civils de Lyon and Claude-Bernard Lyon 1 University, Lyon, France
[s]INSERM UMR 1163, Laboratory of Genome Dynamics in the Immune System, Paris, France
[t]INSERM UMR 1163, Paris, France
[u]Collège de France, Paris, France
*Equal contribution

Corresponding author: Bénédicte Neven, Pediatric Hematology-Immunology and Rheumatology Department, Hôpital Necker-Enfants Malades, 149 rue de Sèvres, 75015 Paris, France. Mail: benedicte.neven@aphp.fr, Phone: + 33 1 44 49 48 22, Fax: + 33 1 44 49 50 70.

Sources of funding: This study was funded by the Institut National de la Santé et de la Recherche Médicale, by the European Research Council, and by the National Research Agency.

Capsule summary

This article demonstrates that JAK inhibition represents a highly promising and well-tolerated therapy for STING-associated vasculopathy, and which may also be relevant to the treatment of other type I interferonopathies.

Key words: Stimulator of Interferon genes, *TMEM173*, Janus kinase 1/2 inhibitor, type I interferonopathy, interstitial lung disease, vasculopathy.

To the Editor:

Gain-of-function mutations in *TMEM173* encoding STING (Stimulator of Interferon Genes) underlie a novel type I interferonopathy,[1] termed SAVI (STING-associated vasculopathy with onset in infancy).[2,3] This disease is associated with high childhood morbidity and mortality. STING is a central component of DNA sensing that leads to the induction of type I interferons (IFN), which in turn drives the expression of IFN-stimulated genes (ISGs) through the engagement of a common receptor and subsequent activation of Janus kinase 1 (JAK1) and tyrosine kinase 2 (TYK2).

We describe, for the first time, the use and efficacy of ruxolitinib, a selective oral JAK1/2 inhibitor, in three children with *TMEM173*-activating mutations over 6 to 18 months of follow-up. The patients, aged between 5 and 12 years, exhibited the phenotypic variability associated with *TMEM173*-activating mutations,[2,3,4] with lung disease and systemic inflammation being the major features in P1 and P3, whilst in P2 skin involvement was most prominent (Fig 1 and see Supplemental Text, Fig E3, and Table E1 in the Online Repository). There was minimal response to a broad spectrum of immunosuppressive therapies including steroids, methotrexate and anti-CD20 monoclonal antibodies.

An increased expression of ISGs, a so-called type I IFN signature,[5] was observed in all three patients (see Fig E1, *A* in the Online Repository). Increased levels of STAT1 phosphorylation were recorded in patient T lymphocytes (P1, P2, P3), T cultured lymphoblasts (P1) and primary fibroblasts (P3) compared to controls (see Fig E2, *A* in the Online Repository). Liu *et al.* demonstrated that, *in vitro*, three JAK1 inhibitors (ruxolitinib, tofacitinib and baricitinib) were able to block the constitutive phosphorylation of STAT1 in lymphocytes from *TMEM173*-mutated patients,[2] and we saw that exposure to ruxolitinib inhibited the constitutive phosphorylation of STAT1 and decreased the expression of IL-6 and 3 ISGs tested in T lymphoblasts from P1 (see Fig E2, *B*, *C* in the Online Repository). Considering the severity of the phenotype and the poor response to conventional immunosuppressive therapies, we hypothesized that JAK1 inhibition would block IFN signaling in the context of activating mutations in *TMEM173*.

We observed a marked positive effect on all aspects of the phenotype in all three treated children. There was a general improvement in patient-reported well-being, a reduction of febrile episodes, an almost complete resolution of the associated cutaneous lesions and a

major improvement in pulmonary function (Fig 1, 2, *A*, *B* and see Supplemental Text, Fig E3, Fig E4, and Tables E1, E2, E3 and E4 in the Online Repository). Concordant with these clinical observations it was possible to taper, and then stop, steroid treatment in all three children. Ruxolitinib concentration was assessed during follow-up and showed peak levels consistent with published pharmacokinetic data (see Tables E5 and E6 in the Online Repository).[6]

Ex vivo experimental data mirrored the favorable clinical effect that we observed. Treatment resulted in a trend to reduction of the IFN score in P1 and P3, whilst there was no significant change in the expression of ISGs in P2 (see Fig E1, *B* in the Online Repository). Pre-treatment transcriptomic analysis of whole blood showed differential expression of 119 genes as compared to healthy controls, including 35 up-regulated ISGs ($P < .05$ and $Q < .25$, see Fig E5, *A*, *B* in the Online Repository). Among these 119 genes, the expression levels of 20 previously up-regulated genes decreased significantly after treatment ($P < .05$, Fig E5, *C* in the Online Repository). This list included genes associated with fever (*IRAK-2, IL18RAP, NFκB1*) and vasculopathy (*ICAM1, NOTCH1*).[2] In *ex vivo* flow cytometry assays, we collected blood from P1, P2 and P3 just before the morning drug intake (H0 equals 12 hours after last dose), and 4 hours after dosing (H4). At H0, when ruxolitinib concentration was minimally raised (see Table E6 in the Online Repository), STAT1 phosphorylation in T lymphocytes from patients was higher than in a healthy control. In contrast, at H4, T lymphocyte STAT1 phosphorylation decreased in all patients (see Fig E6 in the Online Repository). STAT1 phosphorylation dynamics were further explored by *ex vivo* kinetic phosphorylation assays in P2. STAT1 phosphorylation in T lymphocytes and neutrophils from P2 began to decrease at H2, was at the lowest level at H4, increased again at H6, and was at its highest at H10 (Fig 2, *C* and see Fig E7, *A* in the Online Repository). Interestingly, in monocytes from P2 STAT1 phosphorylation showed a similar pattern, but was at its highest level at H8 (Fig 2, *C*). These dynamic changes were also observed in a child with a *TMEM173*-activating mutation in whom ruxolitinib was recently initiated (see the Methods section and Fig E7, *B*, *C* in the Online Repository).

Ruxolitinib was well tolerated, particularly considering the hematological and infectious side effects described in the treatment of myelofibrosis.[7,8] Of importance, we observed no increased incidence of infection in any of the three treated children. In one patient with prominent stigmata of systemic inflammation (P1), an initial improvement was followed by a

relapse when treatment was temporarily stopped (Fig 2, *A* and see Fig E4, *A*, *C*, *D* in the Online Repository). The resolution of these features following reinstatement of the drug further indicates a causal relationship between ruxolitinib administration and the observed improvement. We note that a possible explanation for the intensity of the relapse could relate to a cytokine rebound effect, indicating the need for careful monitoring in the case of treatment interruption. Papillary edema secondary to intracranial hypertension was observed in one patient. It is unclear if this, previously unreported, feature should be considered as a side effect of JAK inhibition. However, this observation indicates the need for careful surveillance fundoscopy in treated patients.

Despite marked clinical improvement, incomplete inhibition of type I IFN signaling likely accounts for the variable reduction in ISG expression and the modest fold-changes in expression observed across a larger number of immune-related genes with ruxolitinib treatment. Such a possibility might explain the absence of increased rate of infection in the treated patients, and also suggests the possibility for increased dosing according to clinical response. Modest and incomplete downregulation of ISG was recently described in splenic B cells of mice treated with tofacitinib, a JAK1/3 inhibitor, with differential signaling effects suggesting currently poorly understood facets of IFN regulation.[9] In this regard, our kinetic *ex vivo* experiments provide insights in the rapid dynamic changes in IFN signaling secondary to JAK1 blockade.

Overall, our findings suggest that JAK inhibition represents a highly promising and well-tolerated therapeutic approach to the multisystem sterile inflammation associated with *TMEM173*-activating mutations, warranting further long-term assessment. Specific inhibitors of JAK1 might be particularly attractive in this context. The potential for irreversible lung damage in STING-related disease indicates that early treatment should be considered in order to avoid progression to pulmonary failure. Considering the recognized phenotypic and pathophysiological overlap, treatment by JAK inhibition may also be relevant to other monogenic type I interferonopathies,[1] and the still wider spectrum of diseases associated with an activation of type I IFN such as subsets of systemic lupus erythematosus and dermatomyositis.[10]

For detailed methods, please see the Methods section in this article's Online Repository.

Marie-Louise Frémond, MD,[a,b,c*]
Mathieu Paul Rodero, PhD,[b,c*]
Nadia Jeremiah, PhD,[b,d]
Alexandre Belot, MD, PhD,[e,f]
Eric Jeziorski, MD,[g]
Darragh Duffy, PhD,[h,i]
Didier Bessis, MD,[j]
Guilhem Cros, MD,[a]
Gillian I Rice, PhD,[k]
Bruno Charbit, MSc,[h]
Anne Hulin, PharmD, PhD,[l]
Nihel Khoudour, MD,[l]
Consuelo Modesto Caballero, MD,[m]
Christine Bodemer, MD, PhD,[b,n]
Monique Fabre, MD,[o]
Laureline Berteloot, MD,[p]
Muriel Le Bourgeois, MD,[q]
Philippe Reix, MD,[r]
Thierry Walzer, PhD,[f]
Despina Moshous, MD, PhD,[a,b,s]
Stéphane Blanche, MD, PhD,[a,b]
Alain Fischer, MD, PhD,[a,b,t,u]
Brigitte Bader-Meunier, MD,[a,b,d]
Fréderic Rieux-Laucat, PhD,[b,d*]
Yanick Joseph Crow, MD, PhD,[b,c,k*]
Bénédicte Neven, MD, PhD,[a,b,d]
*Equal contribution

From the [a]Pediatric Hematology-Immunology and Rheumatology Department, Hôpital Necker-Enfants Malades, AP-HP, Paris, France; [b]Paris Descartes University, Sorbonne-Paris-Cité, Institut Imagine, Paris, France; [c]INSERM UMR 1163, Laboratory of Neurogenetics and Neuroinflammation, Paris, France; [d]INSERM UMR 1163, Laboratory of Immunogenetics of Pediatric Autoimmunity, Paris, France; [e]Pediatric Rheumatology, Nephrology and Dermatology Department, Hospices Civils de Lyon, Lyon, France; [f]CIRI, Centre International

de Recherche en Infectiologie, INSERM, U1111, CNRS UMR5308, Ecole Normale Supérieure de Lyon, Université Lyon 1, Lyon, France; [g]Pediatrics Department, Centre Hospitalier Universitaire de Montpellier, Montpellier, France; [h]INSERM UMR 818, Laboratory of Dendritic Cell Immunobiology, [i]Center for Human Immunology, Institut Pasteur, Paris, France; [j]Dermatology Department, Centre Hospitalier Universitaire de Montpellier, Montpellier, France; [k]Manchester Centre for Genomic Medicine, Institute of Human Development Faculty of Medical and Human Sciences, Manchester Academic Health Sciences Centre, University of Manchester, Manchester, United Kingdom; [l]Pharmacology and Toxicology Laboratory, Hôpital Universitaire Henri Mondor, Créteil, France; [m]Pediatric Rheumatology Department, Hospital Universitari Vall d'Hebron, Barcelona, Spain; [n]Dermatology Department, [o]Pathology Department, [p]Pediatric Radiology Department, [q]Pediatric Pneumology Department, Hôpital Necker-Enfants Malades, AP-HP, Paris, France; [r]Pneumology Department, Centre de Référence de la Mucoviscidose, Hospices Civils de Lyon and Claude-Bernard Lyon 1 University, Lyon, France; [s]INSERM UMR 1163, Laboratory of Genome Dynamics in the Immune System, Paris, France; [t]INSERM UMR 1163, Paris, France; [u]Collège de France, Paris, France.

Acknowledgments

The authors wish to thank the patients and their families for their cooperation in this study. The authors are grateful to Laurie Besson (AE) and Elvira Duchesne (NP) for their technical assistance. Dr Frémond is supported by the Institut National de la Santé et de la Recherche Médicale (Grant number 000427993). Dr Crow acknowledges the European Research Council (GA 309449: Fellowship to Y.J.C), and a state subsidy managed by the National Research Agency (France) under the "Investments for the Future" program bearing the reference ANR-10-IAHU-01.

Conflict of interest

The authors declare no conflict of interest.

References

1. Crow YJ, Manel N. Aicardi-Goutières syndrome and the type I interferonopathies. Nat Rev Immunol. 2015;15:429–40.
2. Liu Y, Jesus AA, Marrero B, et al. Activated STING in a vascular and pulmonary syndrome. N Engl J Med. 2014;371:507–18.
3. Jeremiah N, Neven B, Gentili M, et al. Inherited STING-activating mutation underlies a familial inflammatory syndrome with lupus-like manifestations. J Clin Invest. 2014;124:5516–20.
4. Munoz J, Rodière M, Jeremiah N, et al. Stimulator of Interferon Genes-Associated Vasculopathy With Onset in Infancy: A Mimic of Childhood Granulomatosis With Polyangiitis. JAMA Dermatol. 2015;151:872–7.
5. Rice GI, Forte GMA, Szynkiewicz M, et al. Assessment of interferon-related biomarkers in Aicardi-Goutières syndrome associated with mutations in TREX1, RNASEH2A, RNASEH2B, RNASEH2C, SAMHD1, and ADAR: a case-control study. Lancet Neurol. 2013;12:1159–69.
6. Loh ML, Tasian SK, Rabin KR, et al. A phase 1 dosing study of ruxolitinib in children with relapsed or refractory solid tumors, leukemias, or myeloproliferative neoplasms: A Children's Oncology Group phase 1 consortium study (ADVL1011). Pediatr Blood Cancer. 2015;62:1717–24.
7. Verstovsek S, Mesa RA, Gotlib J, et al. A double-blind, placebo-controlled trial of ruxolitinib for myelofibrosis. N Engl J Med. 2012;366:799–807.
8. Von Hofsten J, Johnsson Forsberg M, Zetterberg M. Cytomegalovirus Retinitis in a Patient Who Received Ruxolitinib. N Engl J Med. 2016;374:296–7.
9. Mostafavi S, Yoshida H, Moodley D, et al. Parsing the Interferon Transcriptional Network and Its Disease Associations. Cell. 2016;164:564–78.
10. Hornung T, Janzen V, Heidgen F-J, Wolf D, Bieber T, Wenzel J. Remission of recalcitrant dermatomyositis treated with ruxolitinib. N Engl J Med. 2014;371:2537–8.

Figures legends

Figure 1: Clinical response of patients with *TMEM173* mutations to treatment with ruxolitinib.

A, High resolution chest CT of P1 demonstrating improvement of ground-glass lesions and stabilization of fibrosis after 12 months (M12) of treatment with ruxolitinib.

B, Cutaneous involvement observed in P2 before (M0), and after 1 (M1) and 16 (M16) months of treatment with ruxolitinib. Healing of the cheek and nose ulcerations was noticed within a month of the initiation of ruxolitinib. Ulcerations of the digits, erythematous scaling plaques of the feet and nail dystrophy improved after 16 months of treatment. These improvements were not related to season (where such lesions are exacerbated by cold and thus are more prominent in the winter and spring months).

Figure 2: CRP levels of P1, disease scores of patients under treatment, and *ex vivo* effect of ruxolitinib.

A, C-reactive protein (CRP) values (normal <2 mg/L, to convert to nmol/L, multiply by 9.524) of P1 are shown before and after treatment with ruxolitinib. Levels of CRP with treatment were found to be significantly decreased compared to levels without treatment (***$P < .001$, Student's t test and see Fig E4, F in the Online Repository). The withdrawal of ruxolitinib, depicted by a dotted line, led to a clinical and biological relapse.

B, Disease scores at screening (M0) and at maximal follow-up (Mmax) (see Methods section in the Online Repository). Disease scores were decreased with treatment in all three patients (see Tables E2, E3, and E4 and Fig E4, C in the Online Repository).

C, PBMCs were obtained from P2 before treatment (H0) and 2, 4, 6, 8, and 10 hours after treatment intake and ruxolitinib concentrations were measured simultaneously. As the treatment is taken twice daily, H0 is at 12 hours after the last dose and immediately before the next dose. Blood from the same healthy control was collected at each time point. STAT1 constitutive phosphorylation quantified in relative mean fluorescent intensity (MFI) in CD3+ lymphocytes and neutrophils began to decrease at H2, was at the lowest level at H4, increased again from H6, and was highest at H10. STAT1 phosphorylation in monocytes showed a comparable pattern but was at maximum at H8. Similar results were observed in CD4+ and CD8+ lymphocytes (see Fig E7, A in the Online Repository).

Figure 1. Clinical response of patients with *TMEM173* mutations to treatment with ruxolitinib.

A

Before treatment

Under treatment (M12)

B

Figure 2. CRP levels of P1, disease scores of patients under treatment, and *ex vivo* effect of ruxolitinib.

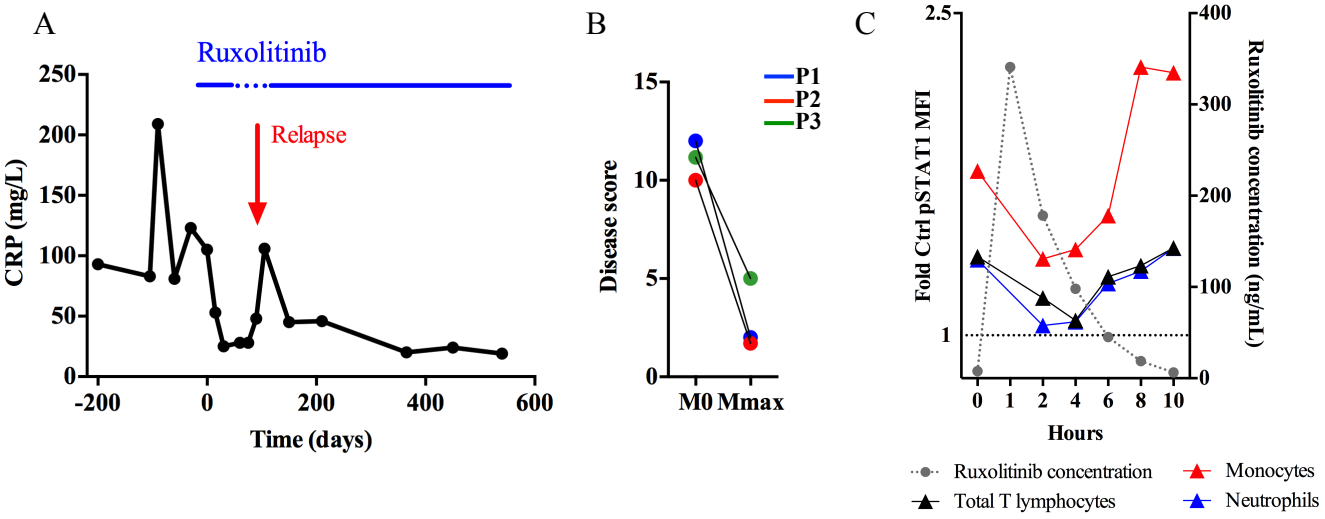

Supplemental Text

EFFICACY OF THE JANUS KINASE 1/2 INHIBITOR RUXOLITINIB IN THE TREATMENT OF VASCULOPATHY ASSOCIATED WITH *TMEM173*-ACTIVATING MUTATIONS IN THREE CHILDREN

Marie-Louise Frémond, MD,[a,b,c*] Mathieu Paul Rodero, PhD,[b,c*] Nadia Jeremiah, PhD,[b,d] Alexandre Belot, MD, PhD,[e,f] Eric Jeziorski, MD,[g] Darragh Duffy, PhD,[h,i] Didier Bessis, MD,[j] Guilhem Cros, MD,[a] Gillian I Rice, PhD,[k] Bruno Charbit, MSc,[h] Anne Hulin, PharmD, PhD,[l] Nihel Khoudour, MD,[l] Consuelo Modesto Caballero, MD,[m] Christine Bodemer, MD, PhD,[b,n] Monique Fabre, MD,[o] Laureline Berteloot, MD,[p] Muriel Le Bourgeois, MD,[q] Philippe Reix, MD,[r] Thierry Walzer, PhD,[f] Despina Moshous, MD, PhD,[a,b,s] Stéphane Blanche, MD, PhD,[a,b] Alain Fischer, MD, PhD,[a,b,t,u] Brigitte Bader-Meunier, MD,[a,b,d] Fréderic Rieux-Laucat, PhD,[b,d*] Yanick Joseph Crow, MD, PhD,[b,c,k*] Bénédicte Neven, MD, PhD,[a,b,d]

[a]Pediatric Hematology-Immunology and Rheumatology Department, Hôpital Necker-Enfants Malades, AP-HP, Paris, France

[b]Paris Descartes University, Sorbonne-Paris-Cité, Institut Imagine, Paris, France

[c]INSERM UMR 1163, Laboratory of Neurogenetics and Neuroinflammation, Paris, France

[d]INSERM UMR 1163, Laboratory of Immunogenetics of Pediatric Autoimmunity, Paris, France

[e]Pediatric Rheumatology, Nephrology and Dermatology Department, Hospices Civils de Lyon, Lyon, France

[f]CIRI, Centre International de Recherche en Infectiologie, INSERM, U1111, CNRS UMR5308, Ecole Normale Supérieure de Lyon, Université Lyon 1, Lyon, France

[g]Pediatrics Department, Centre Hospitalier Universitaire de Montpellier, Montpellier, France

[h]INSERM UMR 818, Laboratory of Dendritic Cell Immunobiology, Institut Pasteur, Paris, France

[i]Center for Human Immunology, Institut Pasteur, Paris, France

[j]Dermatology Department, Centre Hospitalier Universitaire de Montpellier, Montpellier, France

[k]Manchester Centre for Genomic Medicine, Institute of Human Development Faculty of Medical and Human Sciences, Manchester Academic Health Sciences Centre, University of Manchester, Manchester, United Kingdom

[l]Pharmacology and Toxicology Laboratory, Hôpital Universitaire Henri Mondor, Créteil, France

[m]Pediatric Rheumatology Department, Hospital Universitari Vall d'Hebron, Barcelona, Spain
[n]Dermatology Department, Hôpital Necker-Enfants Malades, AP-HP, Paris, France
[o]Pathology Department, Hôpital Necker-Enfants Malades, AP-HP, Paris, France
[p]Pediatric Radiology Department, Hôpital Necker-Enfants Malades, AP-HP, Paris, France
[q]Pediatric Pneumology Department, Hôpital Necker-Enfants Malades, AP-HP, Paris, France
[r]Pneumology Department, Centre de Référence de la Mucoviscidose, Hospices Civils de Lyon and Claude-Bernard Lyon 1 University, Lyon, France
[s]INSERM UMR 1163, Laboratory of Genome Dynamics in the Immune System, Paris, France
[t]INSERM UMR 1163, Paris, France
[u]Collège de France, Paris, France
*Equal contribution

Corresponding author: Bénédicte Neven, Pediatric Hematology-Immunology and Rheumatology Department, Hôpital Necker-Enfants Malades, 149 rue de Sèvres, 75015 Paris, France. Mail: benedicte.neven@aphp.fr, Phone: + 33 1 44 49 48 22, Fax: + 33 1 44 49 50 70.

Sources of funding: This study was funded by the Institut National de la Santé et de la Recherche Médicale, by the European Research Council, and by the National Research Agency.

CONTENTS

I. Supplemental Methods

1. Patients and study approval

Three children from three institutions (Hôpital Necker, Hôpital de Montpellier, and Hospices Civils de Lyon) were recruited. Written informed parental consent was obtained for the use of ruxolitinib on a compassionate basis in all three children. The study and protocols conform to the 1975 Declaration of Helsinki. Written informed consent was obtained for pictures appearing in the manuscript. A fourth patient (P4), an 8-year-old boy carrying a *de novo* p.N154S mutation in *TMEM173* and treated with ruxolitinib for 2 months was included in one experiment (see Fig E7, *B* and *C* in the Online Repository). He is not included in the main text in view of the short treatment time. Consent of the parents and the child was obtained for conducting the experiments.

2. Disease Activity Rating Scale of *TMEM173*-mutated patients

Disease activity was determined at each visit, before and during treatment, according to the rating scale below. The sum of the scores of the 6 components yields the global disease score (range = 0-24).

Fever during the last period:
0: No fever 1: Fever every month 2: Fever every week 3: Fever twice a week 4: Fever every day
Erythematous lesions at visit:
0: No erythematous lesion 1: Erythematous lesions barely present 2: Erythematous lesions covering between 10% and 25% of body surface area 3: Erythematous lesions covering more than 25% of body surface area 4: Erythematous lesions covering more than 25% of body surface area and painful
Ulcer lesions at visit: **The score is calculated for face, left hand, right hand, left foot, right foot, and others regions. The final ulcer score is the sum of the 6 components divided by 6.**

0: No ulcers 1: Few ulcers, no oozing, no ischemia 2: Few ulcers, with some oozing, no ischemia 3: Few ulcers, with significant oozing, and/or any ischemia 4: Multiple ulcers, or with significant oozing and ischemia
Nail and hair lesions at visit:
Nail dystrophy 0: No nail dystrophy 1: Mild and unilateral nail dystrophy 2: Severe or bilateral nail dystrophy Hair lesions 0: No hair lesions 1: Mild thin hair 2: Very thin and breakable hair
Respiratory difficulties during the last period:
0: No dyspnea 1: Mild dyspnea, rapid breathing, but with no functional impact 2: Moderate dyspnea, rapid breathing, with mild functional impact 3: Severe dyspnea, rapid breathing, with severe functional impact (e.g. absence from school) 4: Severe dyspnea, rapid breathing, resulting in staying in bed, oxygen therapy
Fatigue during the last period:
0: No fatigue 1: Mild fatigue, no functional impact 2: Moderate fatigue with mild functional impact 3: Severe fatigue with severe functional impact (e.g. absence from school) 4: Severe fatigue leading to staying in bed most of the time

3. Cell Culture

Peripheral blood mononuclear cells (PBMCs) collected from patients and healthy donors were isolated by Ficoll-Paque density gradient (Lymphoprep, Proteogenix) from blood samples using standard procedures. Expansion of T-cell blasts was performed by incubating PBMCs for 72 hours with phytohaemagglutinin (PHA) (2.5 μg/mL, Sigma-Aldrich) in RPMI 1640

GlutaMax medium (Invitrogen) supplemented with 5% human male AB blood group serum (BioWest), penicillin (100 U/mL) and streptomycin (100 μg/mL). After 3 days, dead cells were removed by Ficoll-Paque density gradient and blasts were maintained in culture with IL-2 (100 U ml/L). Human primary fibroblasts were cultured in Dulbecco's modified Eagle medium (Gibco) supplemented with 10% heat-inactivated fetal calf serum, penicillin (100 U/mL) and streptomycin (100 μg/mL).

4. Gene Expression

IFN Score

Total RNA was extracted from whole blood with a PAXgene (PreAnalytix) RNA isolation kit. RNA concentration was assessed with a spectrophotometer (FLUOstar Omega, Labtech). Quantitative reverse transcription PCR (qPCR) analysis was performed using the TaqMan Universal PCR Master Mix (Applied Biosystems), and cDNA derived from 40 ng total RNA. Using TaqMan probes for *IFI27* (Hs01086370_m1), *IFI44L* (Hs00199115_m1), *IFIT1* (Hs00356631_g1), *ISG15* (Hs00192713_m1), *RSAD2* (Hs01057264_m1), and *SIGLEC1* (Hs00988063_m1), the relative abundance of each target transcript was normalized to the expression level of *HPRT1* (Hs03929096_g1) and *18S* (Hs999999001_s1), and assessed with the Applied Biosystems StepOne software v2.1 and DataAssist software v3.01. For each of the 6 probes, individual (patient and control) data were expressed relative to a single calibrator. IFN scores were calculated from the median fold change in relative quantification values for the set of 6 ISGs, where a score of >2.466 is considered abnormal. The IFN score was calculated for the three patients at screening and at different time-points thereafter.

Gene-Expression Analysis by RNA Hybridization Array

Total RNA extracted from whole blood (as described above) of patients and three healthy controls was diluted with RNase-free water at 20ng/μL, and 100ng (5μL) of each sample was analyzed using the Human Immunology kit v2 and Nanostring nCounter®. Each sample was analyzed in a separate multiplexed reaction including in each, 8 negative probes and 6 serial concentrations of positive control probes. Data was imported into nSolver™ analysis software (version 2.5) for quality checking and normalization of data according to NanoString® analysis guidelines, utilizing positive probes and housekeeping genes. For analysis, mRNA expression levels were log transformed and mean centered per donor (when applicable) prior to hierarchical clustering (Qlucore Omics Explorer version 3.1). A *P* value less than 0.05 and a *Q* value less than 0.25 were considered significant.

qRT-PCR Quantification of Gene Expression

T lymphoblasts were treated or not with ruxolitinib 1 μM for 24 hours at 37°C. Total RNA was extracted using RNAqueous-Micro Kit (Ambio). Reverse transcription was performed using the High-Capacity cDNA Reverse Transcription Kit (Applied Biosystems). Messenger RNAs were quantified by qRT-PCR using Taqman Gene Expression Assay (Applied Biosystems) and normalized to the expression level of *HPRT1*.

5. Pharmacokinetic Studies

A liquid chromatography-tandem mass spectrometry (LC-MS/MS) method, performed by electrospray ionization-triple quadrupole mass spectrometry in positive mode, has been developed and validated for the determination of ruxolitinib in human plasma. After addition of Imatinib-D8 as internal standard and protein precipitation, the supernatant is diluted twice in A:B (50:50). Separation was achieved on Hypersil Gold® PFP column using a gradient elution of 10 mM ammonium formate containing formic acid 0.1% and acetonitrile containing 0.1% formic acid at a flow rate of 0.3 mL/min. The detection of quantification and confirmation ions (397/185.9, 397/158.9) was performed using selected reaction monitoring mode. The standard curve ranged from 1 to 500 ng/mL and was fitted to a 1/x weighted quadratic regression model. The lowest limit of quantification was 1 ng/mL. The method also afforded satisfactory results in terms of sensitivity, specificity, precision (intra- and inter-day RSD from 5.3 to 11.2%) and accuracy (88.9 to 108.9%).

6. STAT Phosphorylation Assay Staining

Ficolled PBMCs, primary fibroblasts and T lymphoblasts were treated or not with ruxolitinib 1 μM for 45 minutes at 37°C. Cells were fixed using pre-warmed BD Cytofix Fixation Buffer (10 minutes at 37°C) and then permeabilized using chilled BD Phosflow Perm Buffer III (30 minutes on ice). Cells were washed twice with PBS supplemented with 5% bovine serum albumin (Sigma) and EDTA (2 mM) and then stained for pSTAT Alexa Fluor® 488 (anti-STAT1 pY701, anti-STAT3 pY705), PE-anti-STAT1 pY701, PE-anti-STAT6 pY641, PE-anti-STAT1, Alexa Fluor® 488 anti-IgG2aκ control isotype and cell surface marker (Alexa Fluor® 750 anti-CD14, PE-Cy™7-CD19, APC-CD3, PerCP-Cy™5.5-CD8) for 1 hour at room temperature. Flow cytometry analysis was performed on a Gallios Beckman Coulter flow cytometer. Results were analyzed using Kaluza software v1.3.

7. Statistics

Analyses were performed with PRISM software (v6 for Macintosh, GraphPad Inc.). Data were tested for normality using the D'Agostino and Pearson test. A *P* value less than 0.05 was considered significant.

II. Supplemental Text

Clinical phenotype of patients and response to treatment

Patient 1 (P1), a 5-year-old girl previously reported by Jeremiah *et al*., carried an inherited heterozygous gain-of-function mutation (p.V155M) in *TMEM173*.[E1] Her disease, starting at a few months of age, was characterized by recurrent fevers every 10 days, chronic fatigue, failure to thrive (weight -2 SD, height -2.9 SD) and tachypnea (see Table E1 in the Online Repository). Skin manifestations have always been limited to occasional erythema of the cheeks. Chest computed tomography (CT) scan demonstrated significant interstitial lung disease (Fig 1, *A* and see Fig E3, *A* in the Online Repository). She exhibited markers of chronic systemic inflammation (see Table E1 in the Online Repository). A positive type I interferon (IFN) signature[E3] was observed repeatedly during several months (see Fig E1, *A* in the Online Repository). There was no apparent response to multiple lines of treatment (including high-dose steroids, mycophenolate mofetil (MMF) and anti-CD20 monoclonal antibodies), initiated beyond the age of 35 months because of recurrent episodes of fever and systemic inflammation persisted, failure to thrive (weight -3 SD, height -3.8 SD) and progression of lung disease with fibrosis on CT scan (see Fig E3, *A* and Table E1 in the Online Repository). Ruxolitinib was introduced at the age of 46 months. MMF was discontinued at this time but steroids were maintained at 0.5 mg/kg/day. The initial dose of ruxolitinib was 2.5 mg twice daily, increased to 5 mg twice daily 1 month later. After 2.5 months of treatment a significant improvement of her general condition was noted, with gain of weight (to -2.5 SD), reduced frequency of fevers, a fall in the level of C-reactive protein (CRP) (Fig 2, *A*) and a decrease of basal respiratory rate. Screening fundoscopy performed at this time revealed papillary edema that was ascribed to intracranial hypertension (cerebrospinal fluid normal, open pressure increased and cerebral magnetic resonance imaging normal), for which she was treated with acetazolamide. Although this feature has not been reported as a side effect of ruxolitinib, the drug was tapered and then stopped over a 10-day period. At this point P1 experienced a recrudescence of her fevers, signs of systemic inflammation increased, and hemoglobin level fell to 4.5 g/dL within three weeks (Fig 2, *A*

and see Fig E4, *D* in the Online Repository). Because of her very poor condition, ruxolitinib was reintroduced at 2.5 mg twice daily. On this dosage regimen her clinical condition rapidly improved again, so that she became steroid independent following progressive tapering of the steroid dose over a period of 5 months. After a total of 18 months of follow-up her general condition was significantly better, she had gained weight (from -3 SD to -1.9 SD), respiratory rate had normalized, and she now experienced only occasional fevers (Fig 2, *B* and see Fig E4, *A*, *B*, *C* and Table E1 in the Online Repository). Regular fundus examinations disclosed a reduction, but persistence, of papillary edema on acetazolamide. A chest CT scan, performed 12 months post initiation of treatment, documented improvement of interstitial pneumonitis and stabilization of fibrosis (Fig 1, *A*). CRP ranged from 10 to 20 mg/L (to convert to nmol/L, multiply by 9.524), and hemoglobin was between 10.5 and 11 g/dL (Fig 2, *A*, and see Fig E4, *D*, *E*, and *F,* and Table E1 in the Online Repository).

Patient 2 (P2), a 9 year-old boy previously reported by Munoz *et al*., was identified to carry a *de novo* p.V147M mutation in *TMEM173*.[E4] He presented from the age of 2 months with severe chronic skin vasculitis involving the feet, hands, nose and cheeks requiring daily opioid therapy, with failure to thrive (weight -2.6 SD, height -4 SD) and minimal pulmonary disease (Fig 1, *B* and see Table E1 in the Online Repository). Recurrent fevers were documented in infancy but progressively disappeared during early childhood. There was no elevation of inflammatory markers. However, a persistent type I IFN signature was detected (see Fig E1, *A* in the Online Repository). He was treated with steroids, MMF, methotrexate, hydroxychloroquine, colchicine, intravenous immunoglobulins and anti-CD20 monoclonal antibodies without apparent clinical benefit. Ruxolitinib was introduced at the age of 8 years, at the initial dose of 2.5 mg twice daily. At this time P2 was treated with steroids at 0.6 mg/kg/day. Improvement of his general condition was noticed within 4 weeks of the initiation of therapy, with obvious resolution of the cutaneous lesions on the cheeks and nose (Fig 1, *B*). Since ruxolitinib tolerance was good, the dose was increased to 5 mg twice daily after 2 months and to 7.5 mg and 10 mg twice daily respectively 3 and 14 months thereafter. Steroids were progressively tapered, and then stopped after 8 months of treatment with ruxolitinib. At last follow-up, 16 months post initiation of ruxolitinib, his general condition was significantly better with no functional impact, associated with a complete resolution of the cutaneous lesions on his hands and face and a marked improvement of the lesions on his feet and observed nail dystrophy (Fig 1, *B*, Fig 2, *B* and see Fig E4, *A*, *B*, *C* and Table E1 in the Online Repository). Papillary edema was excluded on regular fundoscopy, and hematological cell

counts were stable.

Patient 3 (P3), a 12-year-old boy, was identified to carry a maternally inherited p.V155M mutation in *TMEM173*. He presented at the age of 1 year with failure to thrive (weight -2.2 SD, height -1.4 SD), and later tachypnea and chronic cough with digital clubbing and recurrent fevers (see Table E1 in the Online Repository). Features of lung fibrosis were obvious by 5 years of age, and progressed such that he was considered a candidate for lung transplantation 6 years later. Skin involvement became apparent at the age of 11 years, with chilblains of the feet and left ear. Chest CT scan demonstrated severe interstitial and fibrotic lung disease (see Fig E3, *B* in the Online Repository). Lung biopsy revealed centrolobular peribronchiolar polymorphic lymphocytic infiltrate. A 6-minute walking test was severely impaired and associated with tachycardia and desaturations (see Table E1 in the Online Repository). He exhibited a moderate elevation of chronic inflammatory markers, and a marked and persistent IFN signature (see Fig E1, *A* in the Online Repository). He was dependent on nocturnal oxygen, and had previously received hydroxychloroquine, steroids and pulse steroids without obvious efficacy. At the age of 12 years, at which point P3 was treated with hydroxychloroquine and low-dose steroids (0.2 mg/kg/day), ruxolitinib was introduced at the initial dose of 5 mg twice daily. After a follow-up period of 6 months improvement of skin disease and fevers was obvious, accompanied by a decrease of respiratory rate and a gain in weight (Fig 2, *B* and see Fig E3, *C,* Fig E4, *A*, *B*, *C* and Table E1in the Online Repository). The 6-minute walking test was markedly improved, although desaturations still occurred during exercise (see Table E1 in the Online Repository). Steroids were discontinued after 1 month of ruxolitinib treatment. Strikingly, consistent with an improvement of nocturnal oximetry recordings, it was possible to stop nocturnal oxygen therapy after 6 months of ruxolitinib. Chest CT scan at 6 months post initiation of treatment revealed a slight attenuation of the ground-glass appearance of the lower lobes (see Fig E3, *B* in the Online Repository). There was a reduction of the CRP. Tolerance of ruxolitinib was good, allowing for an increase of the dose to 7.5 mg and then 10 mg twice daily. Papillary edema was excluded on fundus examination and hematological cell counts have been stable.

Disease activity score

Disease scores were determined prior to ruxolitinib initiation and during follow-up at each visit. Treatment resulted in a reduction of the disease scores in all three patients (Fig 2, *B*, and see Fig E4, *C*, and Tables E2, E3, and E4 in the Online Repository).

III. Supplemental References

E1. Jeremiah N, Neven B, Gentili M, et al. Inherited STING-activating mutation underlies a familial inflammatory syndrome with lupus-like manifestations. J Clin Invest. 2014;124:5516–20.

E2. Geiger R, Strasak A, Treml B, et al. Six-minute walk test in children and adolescents. J Pediatr. 2007;150:395–9.

E3. Rice GI, Forte GMA, Szynkiewicz M, et al. Assessment of interferon-related biomarkers in Aicardi-Goutières syndrome associated with mutations in TREX1, RNASEH2A, RNASEH2B, RNASEH2C, SAMHD1, and ADAR: a case-control study. Lancet Neurol. 2013;12:1159–69.

E4. Munoz J, Rodière M, Jeremiah N, et al. Stimulator of Interferon Genes-Associated Vasculopathy With Onset in Infancy: A Mimic of Childhood Granulomatosis With Polyangiitis. JAMA Dermatol. 2015;151:872–7.

E5. Schoggins JW, Wilson SJ, Panis M, et al. A diverse range of gene products are effectors of the type I interferon antiviral response. Nature. 2011;472:481-5.

E6. Stojanov S, Lapidus S, Chitkara P, et al. Periodic fever, aphthous stomatitis, pharyngitis, and adenitis (PFAPA) is a disorder of innate immunity and Th1 activation responsive to IL-1 blockade. Proc Natl Acad Sci U S A. 2011;108:7148–53.

E7. Kanakaraj P, Schafer PH, Cavender DE, et al. Interleukin (IL)-1 receptor-associated kinase (IRAK) requirement for optimal induction of multiple IL-1 signaling pathways and IL-6 production. J Exp Med. 1998;187:2073–9.

E8. Liu Y, Jesus AA, Marrero B, et al. Activated STING in a vascular and pulmonary syndrome. N Engl J Med. 2014;371:507–18.

E9. Piggott K, Deng J, Warrington K, et al. Blocking the NOTCH pathway inhibits vascular inflammation in large-vessel vasculitis. Circulation. 2011;123:309–18.

IV. Supplemental Legend Figures

Figure E1: IFN score of *TMEM173*-mutated patients before and during treatment with ruxolitinib.

A, IFN score (normal <2.466) of P1 (n = 1), P2 (n = 2) and P3 (n = 2) before treatment with ruxolitinib reflecting markedly increased expression of IFN induced genes transcripts.

B, IFN score (normal <2.466) at screening and during follow-up. The IFN score in P1 (blue, # indicates the temporary interruption of the treatment) shows a sustained trend to reduction, which was statistically significant (linear regression, slope with $R^2 = .5551$, $P = .01$). There was also a trend towards reduction of the IFN score in P3 (green), but which was not seen in P2 (red).

Figure E2: Constitutive phosphorylation of STAT1 in *TMEM173*-mutated patients and *in vitro* effect of ruxolitinib.

A, Increased constitutive phosphorylation of STAT1 in CD3+ lymphocytes from P1, P2, and P3, and in lymphoblasts from P1 and primary fibroblasts from P3 compared to a healthy control.

B, Decreased constitutive phosphorylation of STAT1, STAT3 and STAT6 in lymphoblasts from P1 treated *in vitro* with ruxolitinib 1 μM. Phosphorylation of STAT1, STAT3 and STAT6 in lymphoblasts from a healthy control was not affected by *in vitro* treatment with ruxolitinib 1 μM.

C, qRT-PCR gene expression analysis in lymphoblasts from P1 and a healthy control, after 24 hours of culture in the presence (empty circles) or absence (filled circles) of ruxolitinib. Results show that *IFIT1*, *IFI27*, *ISG15* and *IL6* were induced in P1 as compared to the control, and levels decreased after *in vitro* treatment.

Figure E3: High-resolution chest computed tomography (CT) imaging performed in *TMEM173*-mutated patients and cutaneous involvement observed in P3 before and during treatment with ruxolitinib.

A, Chest CT of P1 performed at the age of 2.5 years showed bilateral alveolar and interstitial disease with ground-glass lesions and interlobular septa thickening. At the age of 3 years the intensity of the ground-glass lesions had decreased slightly, but fibrosis with pleural and paraseptal cystic lesions and associated bronchiectasis was now clearly evident in the left lower lobe. At screening, aged 4 years, fibrosis had worsened, with retraction of the left lower

lobe. After 12 months of treatment with ruxolitinib the ground-glass lesions were less marked, pulmonary expansion improved and fibrosis stabilized.

B, Chest CT of P3 performed at screening, at the age of 12 years, showing emphysema and honeycombing predominantly located in the middle and upper lobes, reticulation and ground-glass lesions in the lower lobes. After 6 months of treatment with ruxolitinib ground-glass opacities were less marked, whilst emphysema and reticulation – considered as fixed lesions – remained unchanged.

C, Cutaneous involvement observed in P3 before (M0) and after 6 (M6) months of treatment with ruxolitinib, demonstrating healing of the lesions seen on the feet. The improvement observed was not related to season.

Figure E4: Weight and disease scores of *TMEM173*-mutated patients and, hemoglobin and CRP levels of P1 in response to treatment with ruxolitinib.

A, Weight (in standard deviations of the mean) at screening and during follow-up. Treatment with ruxolitinib resulted in a gain in weight in all three patients. Temporal interruption of the treatment in P1 (indicated by #) led to a relapse. Reintroduction of treatment was associated with improved growth.

B, Weight in standard deviation (SD) at screening (M0) and at maximal follow-up (Mmax) showing improved growth in all three patients.

C, Disease scores at screening and during follow-up. Treatment with ruxolitinib improved the disease score in all three patients. The disease score in P1 (blue, # indicates the temporary interruption of the treatment) worsened dramatically during the relapse.

D, Hemoglobin levels of P1 are shown before and after treatment with ruxolitinib. Treatment with ruxolitinib resulted in an increase of hemoglobin. Temporal interruption of the treatment, depicted by a dotted line, led to a clinical and biological relapse. Reintroduction of treatment was associated with a normalization of hemoglobin.

E, F, Hemoglobin values (Panel E) and C-reactive protein (CRP) levels (normal <2 mg/L, to convert to nmol/L, multiply by 9.524) (Panel F) of P1 with and without treatment, at different time points, were compared using Mann-Whitney test and Student's *t* test respectively. Data are presented as means and standard deviations. Levels of CRP with treatment were significantly decreased compared to levels without treatment (***$P < .001$), and hemoglobin levels were significantly higher with treatment (*$P < .01$).

Figure E5: Transcriptomic analysis of *TMEM173*-mutated patients and *ex vivo* effect of ruxolitinib.

A, A heat map showing pre-treatment transcriptomic analysis of whole blood using a panel of 579 immune-related genes, with differential expression of 119 genes as compared to healthy controls ($P < .05$ and $Q < .25$). Among these differentially expressed genes 94 were significantly up-regulated, including 35 ISGs. Fold-changes observed were between -2 and 2. ISG status was determined according to Schoggins *et al.*[E5]

B, The 94 genes up-regulated in the heat map shown in Panel A were classified with respect to their known functional category, according to GeneCards® Human Gene Database (www.genecards.org).

C, A heat map showing the expression of 20 genes up-regulated in all patients prior to treatment, that showed a statistically significant decrease in expression with ruxolitinib therapy ($P < .05$, paired t test). This list included genes associated with fever (*IRAK-2, IL18RAP, NFκB1*)[E6,E7] and vasculopathy (*ICAM1, NOTCH1*).[E8,E9]

Figure E6: *Ex vivo* effect of ruxolitinib on constitutive phosphorylation of STAT1, STAT3 and STAT6 performed in *TMEM173*-mutated patients.

A, B, PBMCs were obtained from P1 before treatment and 4 hours after ruxolitinib intake. As the treatment is taken twice daily, H0 is at 12 hours after the last dose. STAT1, STAT3, and to a lesser extent, STAT6 constitutive phosphorylation in CD3+ lymphocytes (Panel A) was decreased after treatment, being comparable to a healthy control (representative of 2 independent experiments). STAT1 total levels in CD3+ lymphocytes (Panel B) were higher than in the control, before and after treatment.

C, PBMCs were obtained from P2 before treatment and 4 hours after ruxolitinib intake. As the treatment is taken twice daily, H0 is at 12 hours after the last dose. STAT1 constitutive phosphorylation in CD3+ lymphocytes was decreased after treatment.

D, PBMCs were obtained from P3 before treatment and 4 hours after ruxolitinib intake. As the treatment is taken twice daily, H0 is at 12 hours after the last dose. STAT1 and to a lesser extent, STAT3, constitutive phosphorylation in CD3+ lymphocytes was decreased after treatment, being comparable or lower to a healthy control (representative of 2 independent experiments).

Supplemental Tables

	Patient 1		Patient 2		Patient 3	
Age of onset (months)	12		2		12	
Gender	Female		Male		Male	
Mutation of *TMEM173*	p.V155M		p.V147M		p.V155M	
Age at screening (years)	4		8		12	
Follow-up (months)	**At screening**	**18**	**At screening**	**16**	**At screening**	**6**
Disease score (range = 0-24)	12	2	10	1.7	11.2	5
Features of systemic inflammation						
Fever score (range = 0-4)	++++	-	-	-	++	-
Hb (g/dL)	8	11	12	12	12	11.3
CRP (mg/L)	50-100	10-20	6	6	49	19
Failure to thrive: weight (SD), height (SD)	-3, -3.8	-1.9, -3.8	-2.6, -4	-2.4, -3.6	-2.2, -1.4	-1.5, -1.4
Cutaneomucosal lesions scoring						
Erythematous lesions (range = 0-4)	-	-	-	-	++	-
Ulcer lesions (range = 0-4)	-	-	+++	+	+	-
Nails and hair lesions (range = 0-4)	++	-	+++	+	-	-
Pulmonary features						
Respiratory rate (/min)	60	20	30	20	60	32
Interstitial lung disease (on CT)	+++	+*	+	+	+++	++
Fibrosis (on CT)	+	+, stable	-	-	+	+, stable
Altered pulmonary function	++‡ (FRC 188%)	- (FRC 111%)	-	-	+++†	NA¶
Overnight oximetry#	NA	NA	97.3% / 7.4% / 3.8	98.9% / 0.1% / <0.6	91.9% / 7.8% / 0.9	95.8% / 4.3% / <0.6
6MWT (meters)	NA§	351	314§	390§	140**	458
Previous immunosuppressive treatments						
	Steroids, MMF, anti-CD20 monoclonal antibodies		Steroids, MMF, methotrexate, colchicine, hydroxychloroquine, anti-CD20 monoclonal antibodies		Steroids, hydroxychloroquine	
Concomitant treatments at time of initiation of ruxolitinib therapy						
Steroids (mg/kg/day) (time to discontinuation, in months)	0.5	0 (9)	0.6	0 (8)	0.2	0 (1)
Hydroxychloroquine (mg/kg/day)	NA	NA	NA	NA	11	11
Nocturnal supplemental oxygen	-	-	-	-	+	-

Table E1. Summary clinical and laboratory data.

Abbreviations: 6MWT, 6-minute walking test; CRP, C-reactive protein (normal <2 mg/L; to convert to nmol/L, multiply by 9.524); CT, computed tomodensitometry; FRC, functional residual capacity; Hb, hemoglobin; MMF, mycophenolate mofetil; NA, not assessed; SD, standard deviation; Sp02, arterial oxygen saturation measured by pulse oximetry.

6MWT 95% reference ranges in healthy children according to Geiger *et al.*[E2]: female 3 to 5 y: 364.5-692.7 meters; male 6 to 8y: 471.0-659.3 meters; male 9 to 11y: 556.2-801.5 meters; male 12 to 15 y: 600.7-805.3.

*Performed 12 months after initiation of ruxolitinib.

‡Lung distension.

†Severe restrictive lung function.

¶Not assessed because of patient non-compliance.

#Overnight oximetry: mean Sp02, percentage of time with Sp02 < 90%, desaturation index.

§Limited compliance due to reported muscle pains.

**Stop after 2' walk.

Table E2: Disease scores in P1.

	M-6	M-3	M0	M1	M2.5*	M3‡	M6	M12	M18
Fever	4	4	4	3	2	4	0	0	0
Erythematous lesions	0	0	0	0	0	0	0	0	0
Ulcer lesions	0	0	0	0	0	0	0	0	0
Nail and hair lesions	2	2	2	2	2	2	1	0	0
Nail dystrophy	*0*	*0*	*0*	*0*	*0*	*0*	*0*	*0*	*0*
Hair lesions	*2*	*2*	*2*	*2*	*2*	*2*	*1*	*0*	*0*
Respiratory difficulties	3	3	3	2	1	3	1	1	1
Fatigue	3	3	3	2	2	4	2	1	1
Global score	**12**	**12**	**12**	**9**	**7**	**13**	**4**	**2**	**2**

*Indicates the time point before the temporary interruption of treatment with ruxolitinib.
‡Indicates the clinical and biological relapse following temporary cessation of ruxolitinib.

Table E3. Disease scores in P2

	M-6	M-3	M0	M1	M3	M6	M12	M16
Fever	0	0	0	0	0	0	0	0
Erythematous lesions	0	0	0	0	0	0	0	0
Ulcer lesions	3	3	3	2	1.7	1.5	0.8	0.7
Face	*3*	*3*	*3*	*1*	*1*	*1*	*0*	*0*
Left hand	*3*	*3*	*3*	*1*	*1*	*1*	*0*	*0*
Right hand	*3*	*3*	*3*	*1*	*1*	*1*	*0*	*0*
Left foot	*4*	*4*	*4*	*4*	*4*	*3*	*2*	*2*
Right foot	*4*	*4*	*4*	*4*	*3*	*3*	*3*	*2*
Others	*1*	*1*	*1*	*1*	*0*	*0*	*0*	*0*
Nail and hair lesions	3	3	3	3	2	1	1	1
Nail dystrophy	*2*	*2*	*2*	*2*	*1*	*1*	*1*	*1*
Hair lesions	*1*	*1*	*1*	*1*	*1*	*0*	*0*	0
Respiratory difficulties	1	1	1	0	0	0	0	0
Fatigue	3	3	3	2	2	2	1	0
Global score	**10**	**10**	**10**	**7**	**5.7**	**4.5**	**2.8**	**1.7**

Table E4. Disease scores in P3

	M-6	M-3	M0	M1	M3	M6
Fever	2	2	2	1	0	0
Erythematous lesions	2	2	2	1	1	0
Ulcer lesions	0.2	0.2	0.2	0	0	0
Face	*0*	*0*	*0*	*0*	*0*	*0*
Left hand	*0*	*0*	*0*	*0*	*0*	*0*
Right hand	*0*	*0*	*0*	*0*	*0*	*0*
Left foot	*0*	*0*	*0*	*0*	*0*	*0*
Right foot	*0*	*0*	*0*	*0*	*0*	*0*
Others	*1*	*1*	*1*	*0*	*0*	*0*
Nail and hair lesions	0	0	0	0	0	0
Respiratory difficulties	4	4	4	4	4	3
Fatigue	3	3	3	3	2	2
Global score	**11.2**	**11.2**	**11.2**	**9**	**7**	**5**

Table E5: Pharmacokinetic data for ruxolitinib in *TMEM173*-mutated patients.

	Mean H0 (ng/mL)	**Mean H1 (ng/mL)**
P1 (n = 8)	4.032 (0-10.40)	131.6 (33-201.1)
P2 (n = 6)	9.485 (7-14.2)	221.8 (35-341)
P3 (n = 7)	18.63 (1.6-57.9)	174.5 (68.5-362.3)

Concentrations of ruxolitinib 12 hours after treatment (H0) and 1 hour post dosing (H1) in P1, P2 and P3.

Table E6: Pharmacokinetic data for ruxolitinib in *TMEM173*-mutated patients during the STAT phosphorylation assay staining.

	H0 (ng/mL)	**H1 (ng/mL)**	**H4 (ng/mL)**
P1	5.19	94.14	33.3
P2	7.71	341	97.92
P3	1.6	79.8	74.3

Values of ruxolitinib concentrations before ruxolitinib intake corresponding to the residual concentration at 12 hours post dosing (H0), and at 1 (H1) and 4 hours (H4) after treatment intake, measured simultaneously with STAT phosphorylation assay staining (see Fig E6 in the Online Repository).

Figure E1. IFN score of *TMEM173*-mutated patients before and during treatment with ruxolitinib.

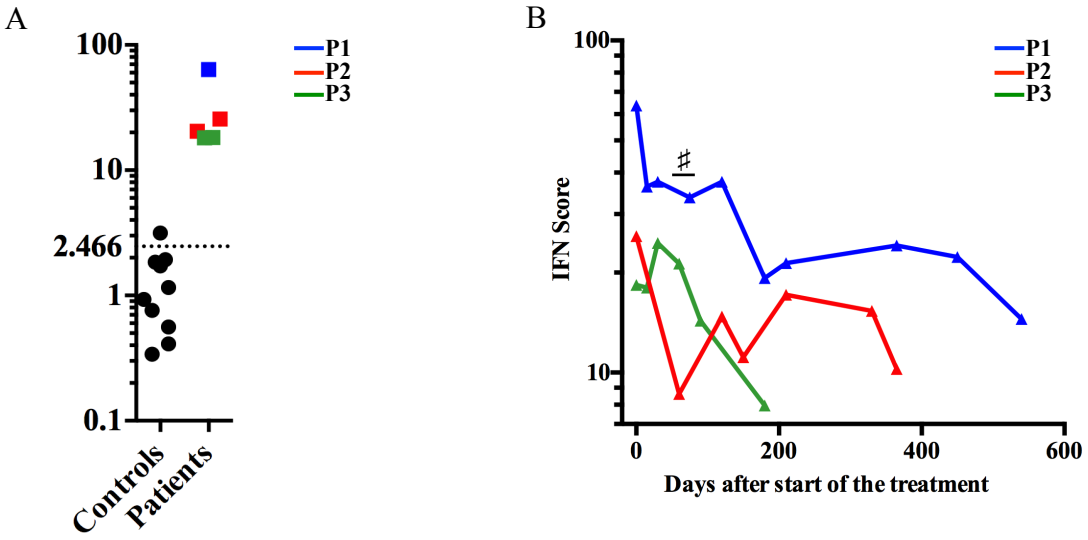

Figure E2. Constitutive phosphorylation of STAT1 in *TMEM173*-mutated patients and *in vitro* effect of ruxolitinib.

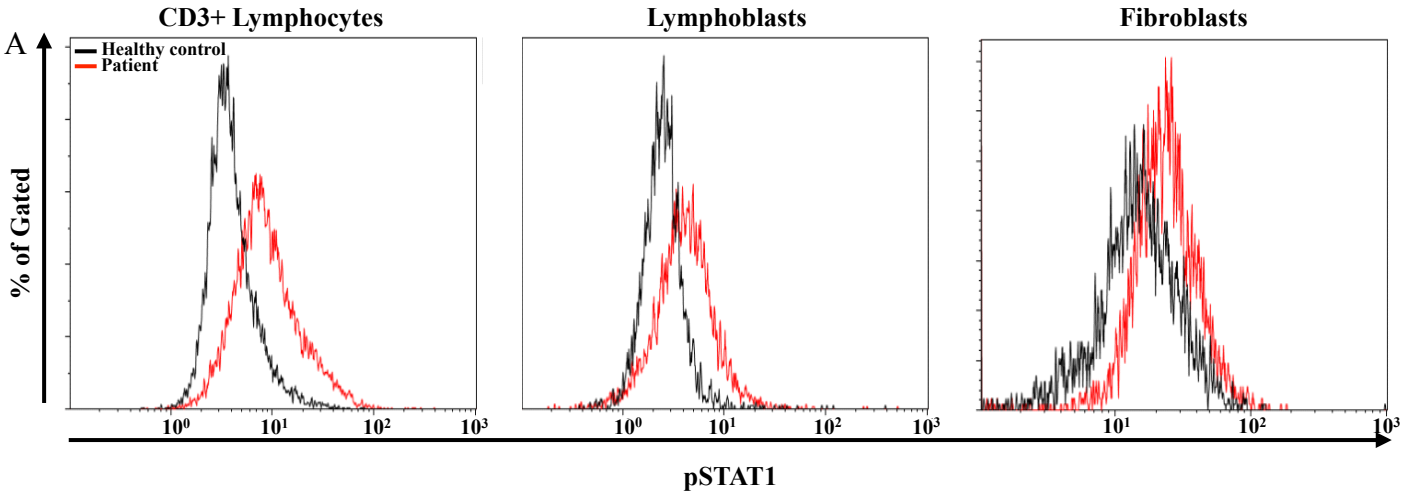

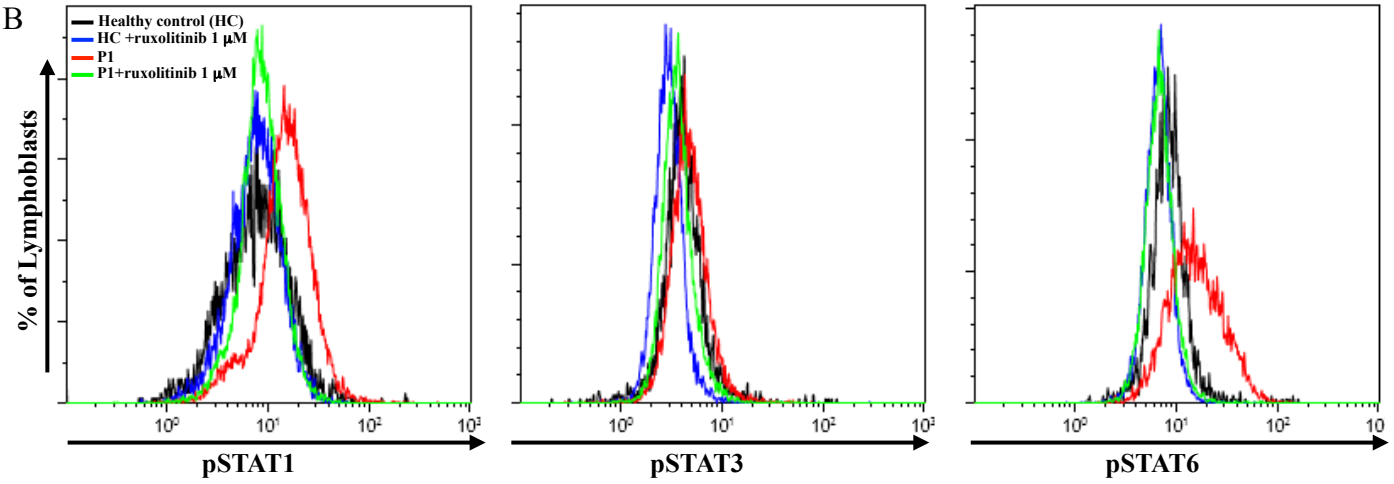

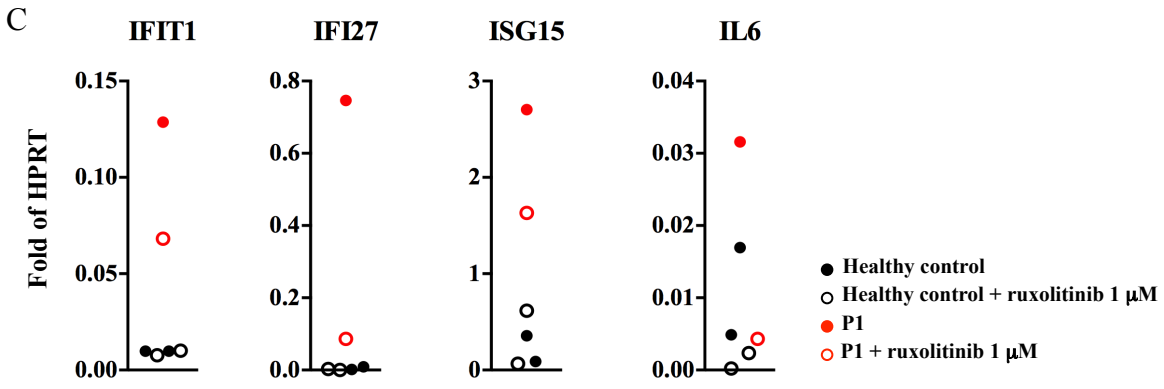

Figure E3. High-resolution chest computed tomography (CT) imaging performed in *TMEM173*-mutated patients and cutaneous involvement observed in P3 before and during treatment with ruxolitinib.

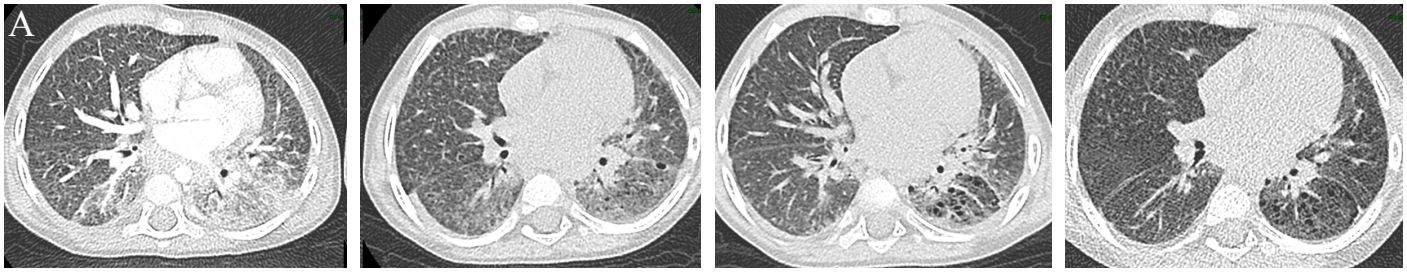

2.5 y | 3 y | 4 y Initiation of treatment | 5 y Under treatment

Before treatment | Under treatment

C

M0 (spring) | M6 (winter)

Figure E4. Weight and disease scores of *TMEM173*-mutated patients, and hemoglobin and CRP levels of P1 in response to treatment with ruxolitinib.

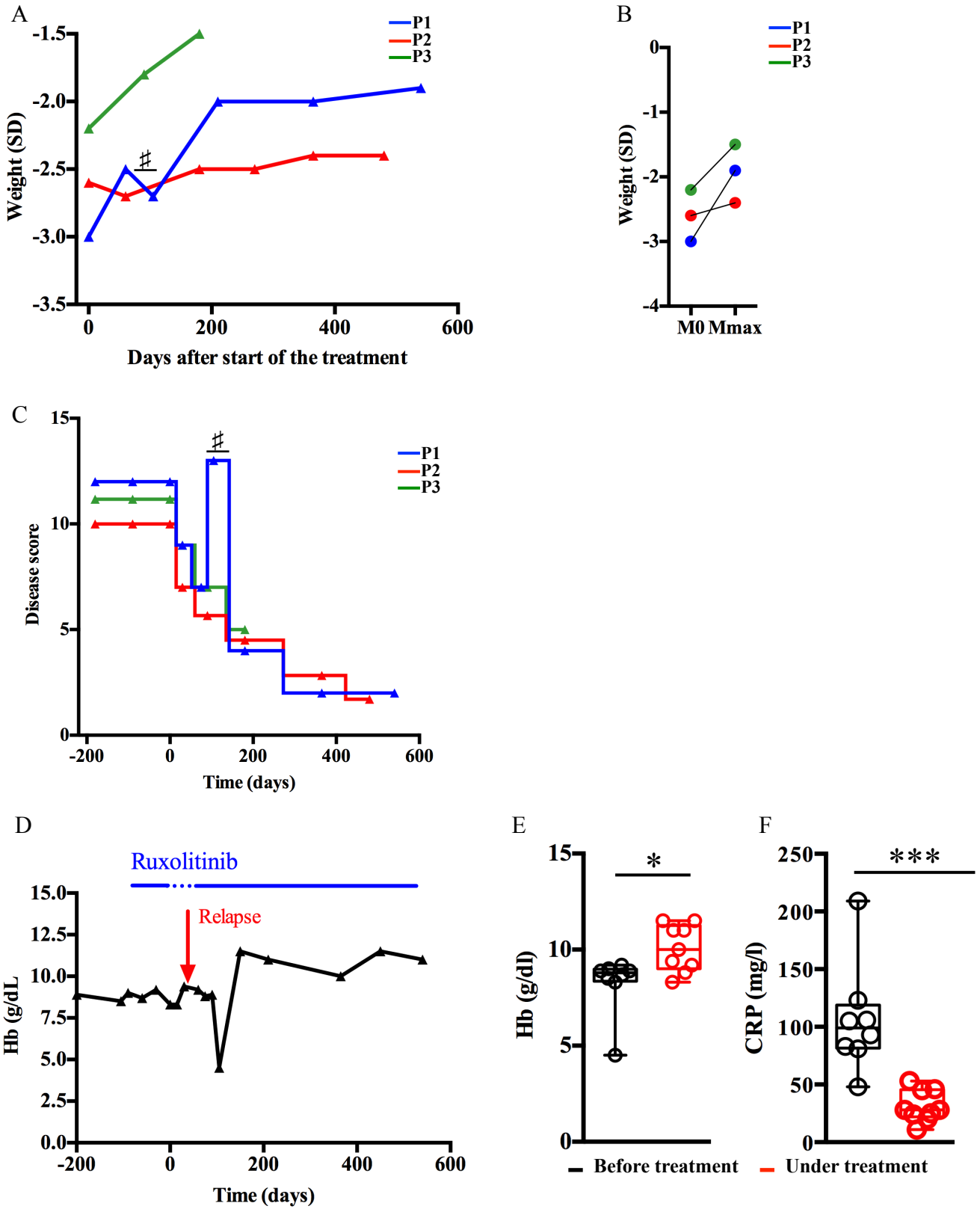

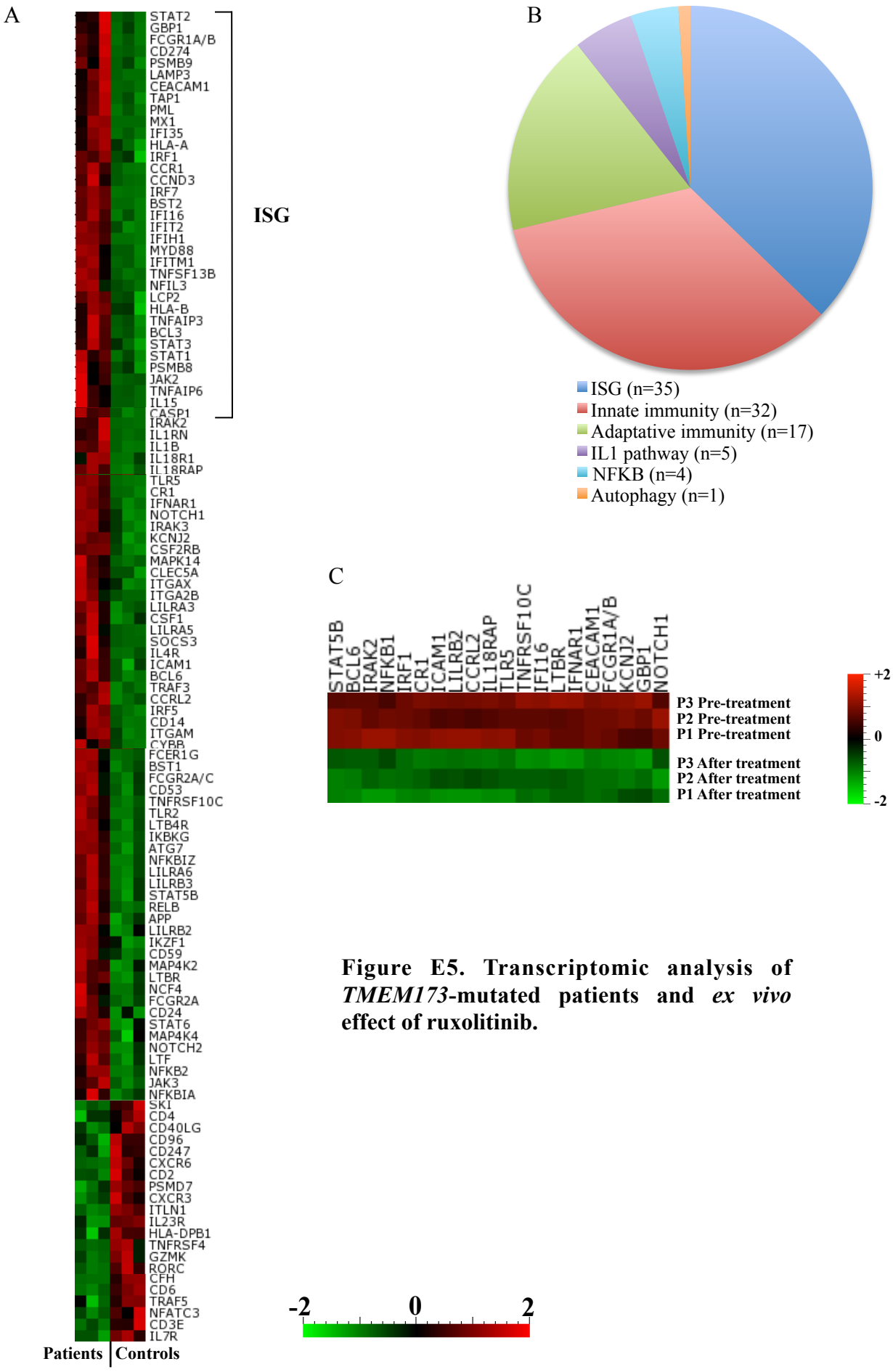

Figure E5. Transcriptomic analysis of *TMEM173*-mutated patients and *ex vivo* effect of ruxolitinib.

Figure E6. ***Ex vivo*** **effect of ruxolitinib on constitutive phosphorylation of STAT1, STAT3 and STAT6 performed in** ***TMEM173*****-mutated patients.**

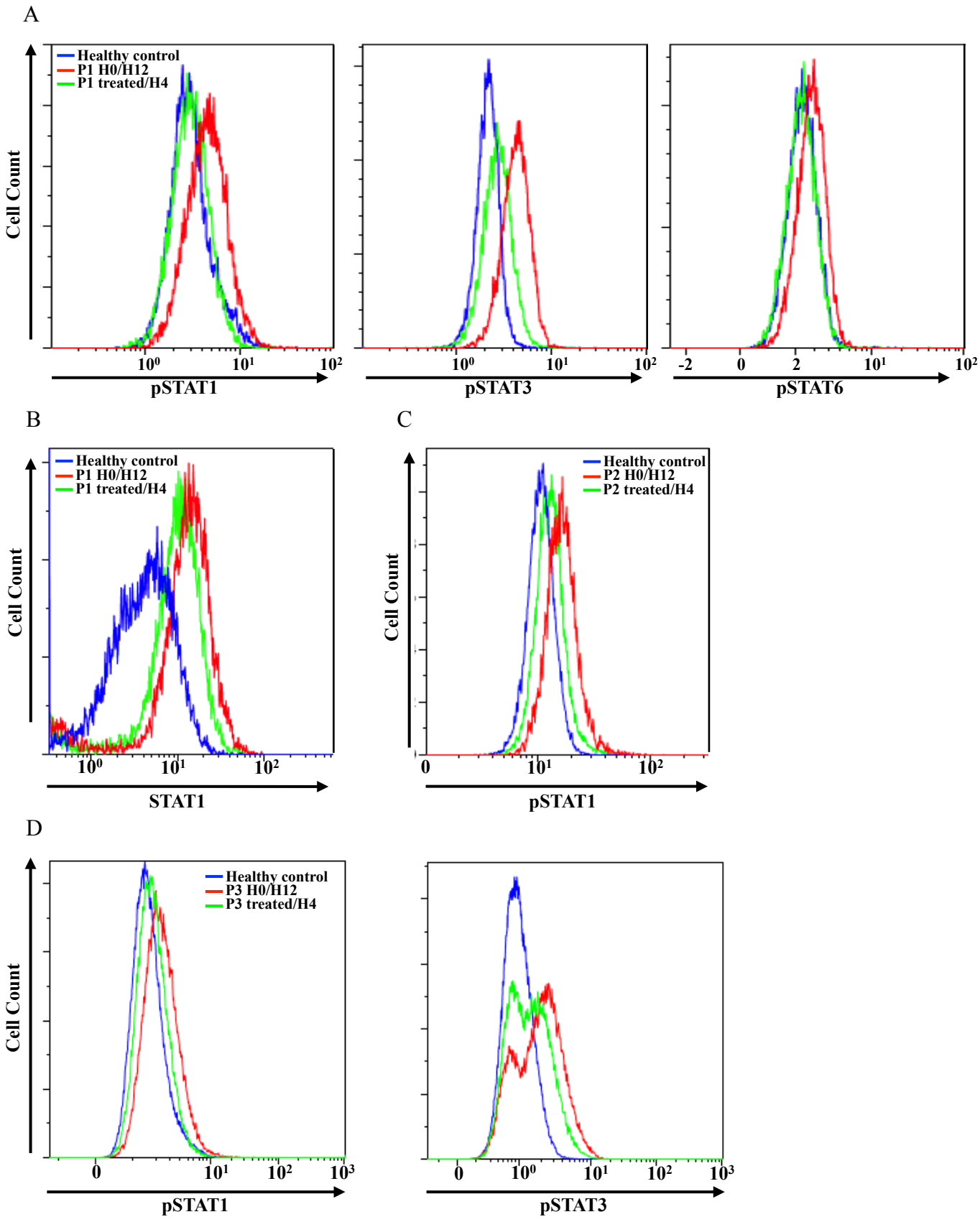

Figure E7. ***Ex vivo*** **kinetic effect of ruxolitinib on constitutive phosphorylation of STAT1 in two** ***TMEM173*****-mutated patients.**

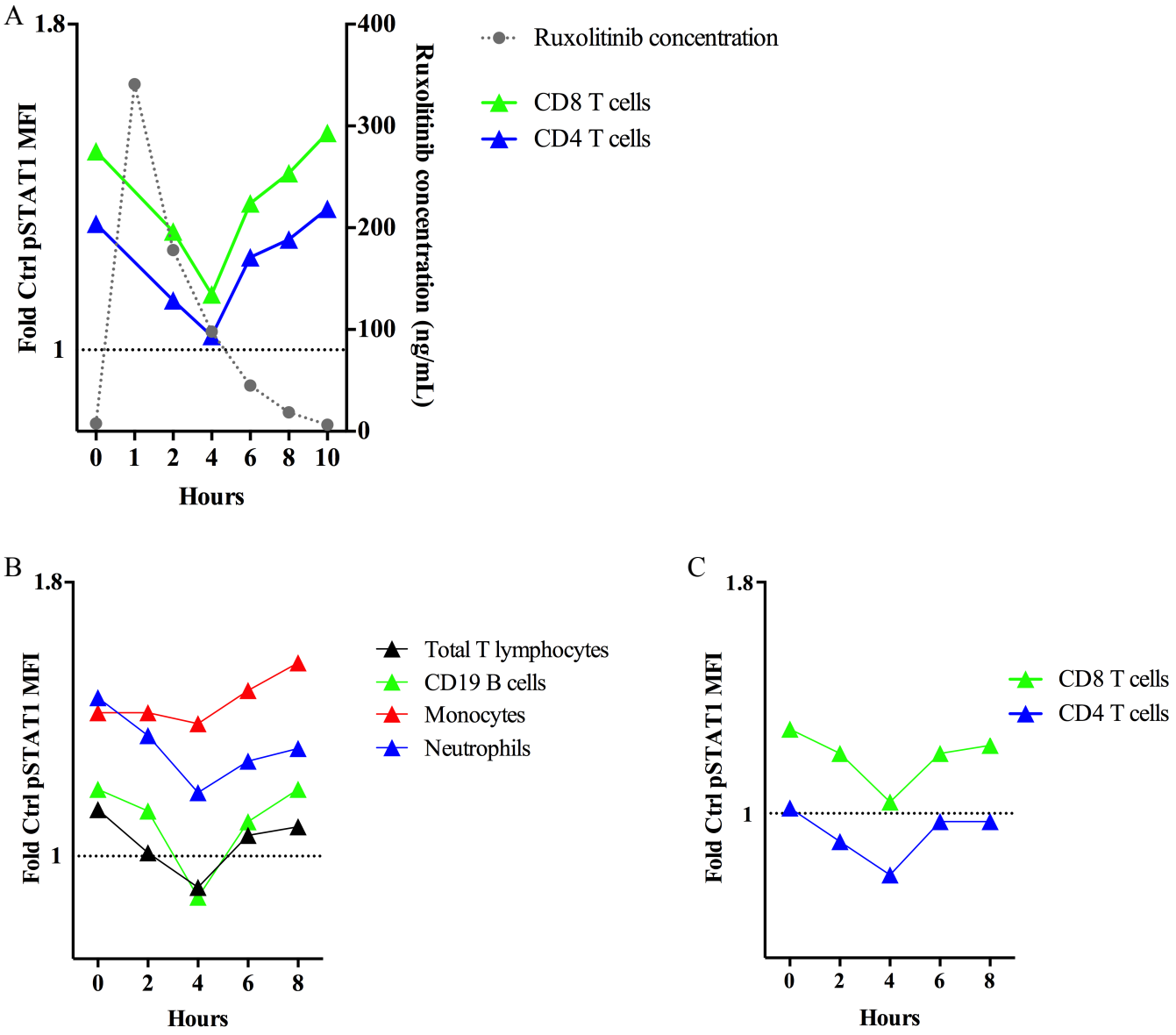

Figure E7: *Ex vivo* kinetic effect of ruxolitinib on constitutive phosphorylation of STAT1 in two *TMEM173*-mutated patients.

PBMCs were obtained from P2 and P4 (see the Methods section in the Online Repository) before treatment and 2, 4, 6, 8 and 10 (P2) hours after ruxolitinib intake. As the treatment is taken twice daily, H0 is at 12 hours after the last dose. Blood from the same healthy control was collected at each time point. The levels of phosphorylation of STAT1 were quantified based on the relative mean fluorescence intensity (MFI) in T lymphocytes, B lymphocytes, monocytes, and neutrophils from P2 and P4 and two healthy controls.

A, STAT1 phosphorylation in CD8+ and CD4+ lymphocytes from P2 began to decrease at H2, was at the lowest level at H4, increased again at H6, and was at its highest at H10.

B, STAT1 phosphorylation in total T lymphocytes, B cells, monocytes, and neutrophils from P4 decreased at H2, was at the lowest level at H4, increased again at H6. STAT1 phosphorylation in monocytes was at its highest level at H8.

C, STAT1 phosphorylation in CD8+ and CD4+ T lymphocytes from P4 showed similar pattern than in panel B.